Slow dynamics of the Northern Hemisphere glaciation

Manfred Mudelsee[1]
Institute of Meteorology, University of Leipzig, Leipzig, Germany

Maureen E. Raymo
Department of Earth Sciences, Boston University, Boston, Massachusetts, USA

Received 10 March 2005; revised 6 September 2005; accepted 16 September 2005; published 14 December 2005.

[1] Unraveling the dynamics of the Northern Hemisphere glaciation (NHG) in the Pliocene is a key step toward a quantitative theory of the climate transition from a greenhouse to an icehouse world. Extracting the ice volume signal from marine oxygen isotope ($\delta^{18}O$) records corrupted with "temperature noise" can be accomplished using statistical time series analysis. We use 45 $\delta^{18}O$ records from benthic and planktonic foraminifera and globally distributed sites to reconstruct the dynamics of NHG initiation. We compare $\delta^{18}O$ amplitudes with those of temperature proxy records and estimate a global ice volume–related increase of 0.4‰, equivalent to an overall sea level lowering of 43 m. We find the NHG started significantly earlier than previously assumed, as early as 3.6 Ma, and ended at 2.4 Ma. This long-term increase points to slow, tectonic forcing such as closing of ocean gateways or mountain building as the root cause of the NHG.

Citation: Mudelsee, M., and M. E. Raymo (2005), Slow dynamics of the Northern Hemisphere glaciation, *Paleoceanography*, *20*, PA4022, doi:10.1029/2005PA001153.

1. Introduction

[2] The Northern Hemisphere glaciation in the Pliocene was a climatic change from a greenhouse world [*Crowley*, 1991] to a world with periodically waxing and waning ice sheets [*Berger et al.*, 1984]. Marine sedimentary records of ice-rafted debris (IRD) and oxygen isotopic composition reveal major glacial expansions at 2.5 Ma [*Shackleton et al.*, 1984] and 2.7 Ma [*Haug et al.*, 1999] ago. (All dates given in this paper refer to the absolutely dated Pliocene timescale in Table 1.) There appear to be two major obstacles to achieving a quantitative and causal understanding of the NHG. First, regarding the size of the glaciation, the $\delta^{18}O$ values record not only changes in ice volume but also changes in regional water temperature [*Shackleton*, 1967]. Second, regarding the timing of the glaciation, the initiation of NHG has not yet been accurately estimated [*Raymo*, 1994]. There were certainly northern glacial episodes in the early Pliocene and Miocene, as documented by IRD events in the Norwegian Sea [*Jansen et al.*, 1990], the Greenland Sea [*Larsen et al.*, 1994], Baffin Bay [*Thiébault et al.*, 1989], and the Fram Strait and Yermak Plateau [*Wolf-Welling et al.*, 1996]. However, a significant increase in global ice volume in the Northern Hemisphere occurred only in the late Pliocene.

[3] In an attempt to quantify the dynamics of the NHG, we employed a simple parametric model of a climate change. Our approach rests on (1) the construction of a large database of $\delta^{18}O$ and temperature records for the interval from 2 to 4 Ma spanning the NHG and (2) the application of statistical time series analysis techniques for signal extraction. By analyzing many records with a quantitative method, we reduce the noise and filter out the ice volume signal. By subtracting the ice volume signal and using calibration formulas, we draw regional maps of temperature changes associated with the NHG. Other dynamical properties of this climate change, such as variability and persistence, are derived. The estimated start and end of the NHG interval help to reduce the set of feasible causal explanations, some of which are discussed here.

2. Data

[4] The database consists of marine proxy records for ice volume and temperature ($\delta^{18}O$, Mg/Ca, faunal assemblages). Because the period of NHG reflects the long-term trend in mean ice volume, coarsely resolved time series can also be utilized.

2.1. Timescale

[5] A new, absolutely dated magnetobiostratigraphic timescale (Table 1) was developed to redate older time series (published before 1994) and erect an accurate time frame for the 2–4 Myr interval. The magnetostratigraphic dates exhibit an excellent agreement with astronomically tuned dates, the average error is ~25,000 years (kyr) [*Mudelsee*, 2005]. Biostratigraphic dates are likely less accurate because of stratigraphic uncertainties and site-specific dependences of the habitats.

2.2. Ice Volume and Temperature Proxy Records

[6] The NHG database (Table 2) includes recently published marine $\delta^{18}O$ time series [*Lisiecki and Raymo*, 2005]. Twenty-five moderate to high-resolution isotope records

[1] Also at Climate Risk Analysis, Halle, Germany.

0883-8305/05/2005PA001153$12.00

Table 1. Pliocene Magnetobiostratigraphic Timescales

Event Number	Event[a]	Type[b]	Absolute Date[c]		Astronomical Tuning,[d] kyr B.P.
			Kiloyears, B.P.	Reference[e]	
1	Olduvai top	M	1776 ± 30	R1	1775
2	Olduvai base	M	1980	R2	1945
3	LAD *D. brouweri*	B			1995
4	Reunion	M	2140 ± 30	R1	
5	FAD acme *D. triradiatus*	B			2170
6	LAD *D. pentaradiatus*	B			2515
7	LAD *D. surculus*	B			2561
8	Matuyama/Gauss	M	2585 ± 50	R3	2600
9	LAD *D. tamalis*	B			2869
10	LAD *G. altispira*	B			3020
11	Kaena top	M	3044 ± 30	interpolation	3046
12	Kaena base	M	3102 ± 51	interpolation	3131
13	LAD *S. seminulina*	B			3160
14	Mammoth top	M	3210 ± 10	R4	3233
15	Mammoth base	M	3300 ± 20	R4	3331
16	Gauss/Gilbert	M	3562 ± 28	interpolation	3594
17	LAD *Sphenolithus spp.*	B			3600
18	LAD *R. pseudoumbilicus*	B			3827
19	S/O *Pulleniatina*	B			3941
20	NN14 base	B			4141
21	Cochiti top	M	4190 ± 20	R5	4185
22	LAD *G. nephentes*	B			4200
23	Cochiti base	M	4260 ± 20	R5	4316
24	Nunivak top	M	4481 ± 14	R5, R6	4479
25	Nunivak base	M	4620 ± 20	R3, R5, R7	4623

[a]Abbreviations are FAD, first appearance date; LAD, last appearance date; NN14, nannoplankton zone 14; S/O, sinistral/dextral coiling change.
[b]Type M is magnetostratigraphic; type B is biostratigraphic.
[c]Errors of absolute ages are 1-σ standard deviations calculated from individual measurement errors. Errors owing to varying age standards or decay constants are neglected. Errors of astronomically tuned ages depend on assumptions made and are not reported.
[d]Tuning is orbital. Magnetostratigraphic dates are averages from dates in ODP Sites 677 [*Shackleton et al.*, 1990], 659 [*Tiedemann et al.*, 1994], and 846 [*Shackleton et al.*, 1995b]. Biostratigraphic dates are averages from dates in ODP Sites 659 [*Tiedemann et al.*, 1994] and 846 [*Shipboard Scientific Party*, 1992], and dates in the compilation by *Berggren et al.* [1995]. Errors of astronomically tuned dates of biostratigraphic events are likely larger than age errors of absolutely dated magnetostratigraphic events.
[e]Sources are R1, *Baksi et al.* [1992]; R2, *Walter et al.* [1991]; R3, *Wilson* [1993]; R4, *Renne et al.* [1993]; R5, *Clement et al.* [1997]; R6, *Hall and Farrell* [1995]; and R7, *Baksi et al.* [1993]. Interpolation was carried out between bracketing magnetostratigraphic dates in Table 1, with the interpolation ratio following the compilation by *Berggren et al.* [1995].

(spacing less than 11 kyr or one half precession cycle) and twenty lower-resolution records (≥11 kyr, or with hiatuses) provide excellent global coverage. Records from benthic foraminifera (29, thereof 18 high-resolution) document changes in global ice volume and bottom water temperature (BWT); planktonic $\delta^{18}O$ data (16, thereof 7 high-resolution) record ice volume and sea surface temperature (SST). Only four temperature proxy time series (from faunal assemblages and Mg/Ca techniques) are available for the 2–4 Myr interval (Table 2).

3. Methods

3.1. Regression

[7] We employed a simple parametric model of a climate change, a "ramp" [*Mudelsee*, 2000], to infer the start, end, and amplitude of the increase in mean $\delta^{18}O$ and temperature from 2–4 Myr. Superimposed on this long-term (>1 Myr) trend are fluctuations, which come mainly from short-term (≤41 kyr) variations in ice volume and temperature. Such variations are partly induced by changes in the Earth's orbital parameters obliquity and precession [*Berger et al.*, 1984]. Salinity effects [*Whitman and Berger*, 1992] and measurement uncertainties add some additional "noise." To estimate the resultant uncertainties of the NHG parameters, start, end, and amplitude, we used extensive computer simulations that take data noise into account.

[8] Fits of the ramp regression model to the $\delta^{18}O$ and temperature time series used a weighted least squares criterion for determining the amplitude combined with a brute force search for determining start and end [*Mudelsee*, 2000]. The increase in variability (time-dependent standard deviation, $\sigma(t)$) across the NHG was quantified by means of a running window. This allows not only to determine the weighting for the regression, but also to measure how much the size of the $\delta^{18}O$ fluctuations increased as the ice sheets grew.

[9] We estimated the persistence time, τ, of $\delta^{18}O$ fluctuations by the decay period of the autocorrelation function [*Mudelsee*, 2002] fitted to the standardized regression residuals (a residual is given by the difference between the $\delta^{18}O$ value and the ramp model value, divided by $\sigma(t)$). To detect outliers (positive and negative $\delta^{18}O$ extremes), we adopted a $\pm 3\ \sigma(t)$ threshold.

[10] We performed computer simulations [*Efron and Tibshirani*, 1993; *Mudelsee*, 2000] as follows to derive parameter uncertainties: (1) Take fitted ramps, $\sigma(t)$ and τ to produce a simulated time series with a random number generator. (2) Fit ramp to simulated data to obtain simulated

Table 2. Database

Record Site	Location		Water Depth m	Description (Foraminifera, Proxy Technique, Temperature Variable[a])	s[b], cm kyr^{-1}	d[c], kyr	References[d]	
	Latitude	Longitude					Data[e]	Timescale[f]
				Benthic $\delta^{18}O$ Records				
V28–179	4°37′N	139°36′W	4509	*G. subglobosa*	0.45	32.2	R1	2, 8, 11, 12, 14, 15, 16
DSDP 397	26°50′N	15°10′W	2900	mainly *U. peregrina*	7.5	35.2	R2	2, 4, 8, 11, 12, 14, 15, 16, 21[g]
DSDP 502	11°29′N	79°23′W	3051	*Cibicidoides* spp.	2.8	28.5	R3, R4	11, 12, 14, 15, 16, 21, R4[h]
DSDP 552	56°03′N	23°14′W	2311	*Cibicidoides* spp.	1.4	9.2	R5, R6	this work[i]
DSDP 586	0°30′S	158°30′E	2218	*C. wuellerstorfi*	2.8	78.2	R7	1, 8, 10, 16, 19
DSDP 586	0°30′S	158°30′E	2218	*O. umbonatus*	2.8	65.5	R7	1, 8, 10, 16, 19
DSDP 590	26°07′S	161°14′E	1533	*C. kullenbergi*	2.8	66.2	R8	2, 8, 11, 15, 16, 20[j]
DSDP 606	37°20′N	35°30′W	3007	*G. subglobosa*	4.2	10.7	R9	2, 4, 8, 11, 12, 14, 15, 16, 21[k]
DSDP 606	37°20′N	35°30′W	3007	*P. wuellerstorfi*	4.2	10.7	R9	2, 4, 8, 11, 12, 14, 15, 16, 21[k]
DSDP 607	41°00′N	32°58′W	3427	*Cibicidoides* spp.	4.2	4.2	R10, R11, R12	Table 1[l]
DSDP 610	53°13′N	18°53′W	2417	*Cibicidoides* spp.	3.4	5.6	R13	4, 8, 11, 12, 14, 15, 16, 21
ODP 659	19°05′N	21°02′W	3070	*C. wuellerstorfi*	2.8	4.1	R14	see data
ODP 662	1°23′S	11°44′W	3821	*Cibicidoides* spp.	4.3	3.5	R12	3, 5, 6, 7, 9, 17[m,n]
ODP 704	46°53′S	7°25′E	2532	*Cibicidoides* spp.	3.0	8.0	R15	2, 4, 11, 12, 14, 15, 16, 21[o]
ODP 722	16°37′N	59°48 E	2028	*Uvigerina* spp	2.7	7.7	S. Clemens (unpublished data, 2004)	R16
ODP 758	5°23′N	90°21′E	2925	*C. wuellerstorfi*	1.3	7.4	R17	2, 8, 11, 12, 14, 15, 16, 21[k]
ODP 806	0°19′N	159°22′E	2520	*C. wuellerstorfi*	3.3	3.3	T. Bickert (unpublished data, 2004)	see data[l]
ODP 846	3°06′S	90°49′W	3296	mainly *C. wuellerstorfi*, *Uvigerina* spp.	4.1	2.4	R18	R19
ODP 849	0°11′S	110°31′W	3851	*C. wuellerstorfi*, *Uvigerina* spp.	2.7	4.0	R20	R19
ODP 925	4°12′N	43°29′W	3040	*Cibicidoides* spp.	3.1	4.3	R21, R22, R23	see data
ODP 927	5°28′N	44°28′W	3326	*Cibicidoides* spp.	3.3	4.5	R21, R22[p]	see data
ODP 929	5°56′N	43°44′W	4361	*Cibicidoides* spp.	2.7	4.5	R21, R22, R23	see data
ODP 982	57°31′N	15°53′W	1145	*C. wuellerstorfi*	2.7	3.2	R12, R24	Table 1[l]
ODP 999	12°44′N	78°44′W	2828	*C. wuellerstorfi*	3.0	3.8	R25	see data
ODP 1014	32°49′N	119°58′W	1177	*C. mckannai*	9.8	19.5	R26	R27[m]
ODP 1018	36°59′N	123°17′W	2467	*C. wuellerstorfi*	9.8	19.7	R26	R27[m]
ODP 1085	29°22′S	13°59′E	1725	*C. wuellerstorfi*	5.3	2.0	R28, R29	see data
ODP 1143	9°22′N	113°17′E	2772	*C. wuellerstorfi*, *U. peregrina*	3.5	3.0	R30	see data
ODP 1148	18°50′N	116°34′E	3294	*Cibicidoides* spp., *Oridorsalis* spp., *Uvigerina* spp.	2.5	7.5	R31	see data
				Planktonic $\delta^{18}O$ Records				
DSDP 572	1°26′N	113°51′W	3893	*G. sacculifer*	1.4	7.7	R32	see data[q]
DSDP 586	0°30′S	158°30′E	2218	*G. sacculifer*	2.8	56.5	R7	1, 8, 10, 16, 19
DSDP 586	0°30′S	158°30′E	2218	*Pulleniatina* spp.	2.8	56.5	R7	1, 8, 10, 16, 19
DSDP 590	26°07′S	161°14′E	1533	*G. sacculifer*	5.3	55.7	R8	2, 8, 11, 15, 16, 20[j]
DSDP 606	37°20′N	35°30′W	3007	*G. bulloides*	4.2	7.9	R9	2, 4, 8, 11, 12, 14, 15, 16, 21[k]
ODP 625	28°50′N	87°10′W	889	*G. ruber*, *G. sacculifer*	3.7	4.3	R33	3, 6, 7, 13, 17, 18, 22[m]
ODP 704	46°53′S	7°25′E	2532	*G. bulloides*, *N. pachyderma*	3.0	6.0	R15	2, 4, 11, 12, 14, 15, 16, 21[o]
ODP 722	16°37′N	59°48′E	2028	*G. sacculifer*	2.7	12.1	R15	see data[r]
ODP 758	5°23′N	90°21′E	2925	*G. sacculifer*	1.3	7.1	R34, R35	2, 8, 11, 12, 14, 15, 16, 21[k]

Table 2. (continued)

Record Site	Location		Water Depth m	Description (Foraminifera, Proxy Technique, Temperature Variable[a])	s[b], cm kyr^{-1}	d[c], kyr	References[d]	
	Latitude	Longitude					Data[e]	Timescale[f]
ODP 806	0°19′N	159°22′E	2520	*G. sacculifer*	3.3	3.5	R36	T. Bickert (personal communication, 2004)[l]
ODP 851	2°46′S	110°34′W	3760	*G. sacculifer*	1.9	5.2	R37	see data[l]
ODP 851	2°46′S	110°34′W	3760	*G. tumida*	1.9	5.1	R37	see data[l]
ODP 851	2°46′S	110°34′W	3760	*N. humerosa*, *N. dutertrei*	1.9	6.7	R37	see data[l]
ODP 925	4°12′N	43°29′W	3040	*G. sacculifer*	3.1	4.6	R22, R38, R39[s]	see data
ODP 999	12°44′N	78°44′W	2828	*G. sacculifer*	3.0	3.2	R40	see data
ODP 1148	18°50′N	116°34′E	3294	*G. ruber*, *G. sacculifer*[t,u]	2.5	9.8	R31	see data
				Temperature Proxy Records				
DSDP 572	1°26′N	113°51′W	3893	Ostracoda assemblages, SST	1.4	18.2	R41	see data[q]
DSDP 607	41°00′N	32°58′W	3427	Mg/Ca benthic foraminifera, BWT	4.2	7.9	R42	Table 1[l]
ODP 806	0°19′N	159°22′E	2520	Planktonic foraminifera assemblages,[v] SST	3.3	7.7	R43	T. Bickert (personal communication, 2004)[l]
ODP 806	0°19′N	159°22′E	2520	Mg/Ca benthic foraminifera, BWT	3.3	254	R44	see data

[a]SST, sea surface temperature; BWT, bottom water temperature.

[b]Average sedimentation rate within regression time interval.

[c]Average temporal spacing within regression time interval.

[d]R*1*, *Shackleton and Opdyke* [1977]; R*2*, *Shackleton and Cita* [1979]; R*3*, *Keigwin* [1982b]; R*4*, *Oppo et al.* [1995]; R*5*, *Shackleton and Hall* [1984]; R*6*, *Curry and Miller* [1989]; R*7*, *Whitman and Berger* [1992]; R*8*, *Elmstrom and Kennett* [1986]; R*9*, *Keigwin* [1986]; R*10*, *Raymo et al.* [1989]; R*11*, *Raymo* [1992]; R*12*, *Lisiecki and Raymo* [2005]; R*13*, *Raymo et al.* [1992]; R*14*, *Tiedemann et al.* [1994]; R*15*, *Hodell and Venz* [1992]; R*16*, *Clemens et al.* [1996]; R*17*, *Chen et al.* [1995]; R*18*, *Shackleton et al.* [1995a]; R*19*, *Shackleton et al.* [1995b]; R*20*, *Mix et al.* [1995]; R*21*, *Bickert et al.* [1997]; R*22*, *Franz* [1999]; R*23*, *Billups et al.* [1998a]; R*24*, *Venz and Hodell* [2002]; R*25*, *Haug and Tiedemann* [1998]; R*26*, *Kwiek and Ravelo* [1999]; R*27*, *Lyle et al.* [2000]; R*28*, *Andreasen* [2001]; R*29*, *Ravelo et al.* [2004]; R*30*, *Tian et al.* [2002]; R*31*, *Jian et al.* [2003]; R*32*, *Prell* [1985]; R*33*, *Joyce et al.* [1990]; R*34*, *Farrell and Janecek* [1991]; R*35*, *Chen* [1994]; R*36*, *Jansen et al.* [1993]; R*37*, *Cannariato and Ravelo* [1997]; R*38*, *Chaisson and Ravelo* [1997]; R*39*, *Billups et al.* [1998b]; R*40*, *Haug et al.* [2001]; R*41*, *Hays et al.* [1989]; R*42*, *Dwyer et al.* [1995]; R*43*, *Andersson* [1997]; R*44*, *Lear et al.* [2003].

[e]Benthic isotope data were adjusted to seawater equilibrium using corrections given by *Shackleton and Hall* [1984] or data references. Planktonic isotope data were adjusted to correct for species variations within a record, see data references.

[f]Given numbers refer to events in Table 1, using absolute dates for magnetostratigraphic events (unless otherwise noted) and astronomically tuned dates for biostratigraphic events. For each record, data, and timescale references (or references cited therein) contain further information on magnetobiostratigraphy and tuning procedure. The average error between records owing to varying timescales (Table 1) is approximately 25 kyr [*Mudelsee*, 2005]. Records with hiatuses or a low time resolution can have significantly larger timescale errors (approximately 100 kyr).

[g]Timescale uncertain in late part.

[h]Combined record was constructed from low-resolution, absolutely dated part (< 2600 kyr) and high-resolution, tuned part (> 2600 kyr). A hiatus exists between 2188 and 2366 kyr.

[i]Using astronomical dating for the interval up to 2100 kyr and magnetostratigraphic events Kaena Base and Gauss/Gilbert on the *Cande and Kent* [1992] timescale for the older interval. Hiatuses exist between approximately 2200 and 2300 kyr and between approximately 2700 and 2828 kyr.

[j]Timescale uncertain in early part.

[k]Ages in early part (at around MIS M2 to MG2) are approximately 50 kyr younger than ages in standard astronomically tuned timescales [*Tiedemann et al.*, 1994; *Shackleton et al.*, 1995b].

[l]Timescale tuned to timescale of *Shackleton et al.* [1995b].

[m]Timescale based wholly on biostratigraphy.

[n]Biostratigraphic timescale correlated to standard astronomically tuned timescales [*Tiedemann et al.*, 1994; *Shackleton et al.*, 1995b] at around MIS 96–98–100.

[o]Hiatus exists between approximately 2240 and 2700 kyr.

[p]Hiatus exists between approximately 3278 and 3530 kyr.

[q]The initial timescale was based on correlation of carbonate records between DSDP Sites 572 and 573 [*Prell*, 1985]; for DSDP 573 a magnetostratigraphy exists (events 2, 8, 11, 12, 14, 15, 16, and 21 in Table 1). The late part of the record (at around MIS 96–98–100) was subsequently correlated with standard astronomically tuned timescales [*Tiedemann et al.*, 1994; *Shackleton et al.*, 1995b].

[r]Hiatus exists between approximately 2846 and 3323 kyr.

[s]Very low resolution between 2 and approximately 2.6 Ma.

[t]*G. ruber* was used in interval from 2 Ma to approximately 3.1 Ma; *G. sacculifer* was used in interval from approximately 3.1 to 4 Ma.

[u]Low resolution between approximately 3 and 4 Ma.

[v]Modern analog technique.

Table 3. Results[a]

Record[b]	Start, kyr	End, kyr	$\delta^{18}O$ Amplitude, ‰	Cooling, °C	τ, kyr
		Benthic Records			
606 b *G.s.*	3506 ± 253	2753 ± 293	0.47 ± 0.12	0.4 ± 0.7	8.7 ± 2.0
606 b *P.w.*	3440 ± 264	2545 ± 309	0.61 ± 0.13	1.2 ± 0.7	6.3 ± 1.5
607 b	2903 ± 106[c]	2720 ± 125	0.53 ± 0.06	0.62 ± 0.29	10.9 ± 1.4
610 b	3347 ± 238	2831 ± 204	0.41 ± 0.09	0.1 ± 0.5	6.6 ± 1.0
659 b	3459 ± 222	2084 ± 273[d]	0.52 ± 0.09	0.7 ± 0.5	6.3 ± 0.8
662 b	3191 ± 200	2463 ± 216	0.58 ± 0.13	1.0 ± 0.7	12.9 ± 2.2
722 b	3499 ± 195	2077 ± 221[d]	0.49 ± 0.07	0.5 ± 0.4	5.0 ± 0.9
758 b	3502 ± 192	2150 ± 196	0.54 ± 0.07	0.8 ± 0.4	8.0 ± 1.3
806 b	3695 ± 160	2639 ± 190	0.44 ± 0.06	1.0 ± 0.5	7.3 ± 0.8
846 b	3700 ± 160	2462 ± 200	0.60 ± 0.07	1.1 ± 0.4	8.0 ± 0.9
849 b	3176 ± 99	2446 ± 198	0.51 ± 0.07	0.7 ± 0.4	10.4 ± 1.3
925 b	2732 ± 187[c]	2532 ± 177	0.37 ± 0.07	−0.1 ± 0.4	6.4 ± 0.8
929 b	3747 ± 189	2930 ± 212	0.51 ± 0.08	0.7 ± 0.4	8.4 ± 1.0
982 b	3827 ± 193[d]	2095 ± 200[d]	0.47 ± 0.06	0.4 ± 0.3	7.9 ± 0.9
999 b	3861 ± 153[d]	2090 ± 195[d]	0.54 ± 0.06	0.8 ± 0.3	7.0 ± 0.8
1085 b	3777 ± 147	2168 ± 193	0.53 ± 0.06	1.0[e]	7.1 ± 0.8
1143 b	3613 ± 138	2172 ± 165	0.69 ± 0.08	1.6 ± 0.4	5.4 ± 0.6
1148 b	3734 ± 146	2492 ± 166	0.68 ± 0.07	1.6 ± 0.4	7.5 ± 1.4
		Planktonic Records			
572 p	3152 ± 177	2830 ± 183	0.36 ± 0.06	0.12 ± 0.47	9.3 ± 1.5
606 p	3760 ± 216	2001 ± 254[d]	0.42 ± 0.06	0.2 ± 0.3	4.3 ± 0.9
625 p	3992 ± 406[d]	2013 ± 378[d]	0.39 ± 0.07	0.0 ± 0.4	4.2 ± 0.5
758 p	3050 ± 110	2692 ± 127	0.38 ± 0.04	−0.1 ± 0.2	5.7 ± 0.9
806 p	3936 ± 147[d]	2000 ± 200[d]	0.27 ± 0.04	−0.85 ± 0.17	3.0 ± 0.3
851 p *G.sac.*	3584 ± 236	2429 ± 225	0.51 ± 0.08	0.7 ± 0.4	6.5 ± 0.8
999 p	3587 ± 188	2504 ± 193	0.46 ± 0.07	0.4 ± 0.4	4.5 ± 0.5
Average[f]	3606 ± 60[g]	2384 ± 64[g]			7.1 ± 0.4[h]

[a]The high-resolution records were analyzed to obtain NHG parameters start, end, $\delta^{18}O$ amplitude within interval 2384–3606 kyr, and persistence time, τ. For the records 572 p, 607 b, 806 b, 806 p, and 1085 b the cooling of the water masses during this interval was determined via proxies (Figure 3). For the other records it was estimated by subtracting an ice volume signal of 0.39‰ from the $\delta^{18}O$ amplitudes and using the $\delta^{18}O$ temperature calibrations (section 3.2). Persistence time average results from using values from benthic records only.

[b]Caption for Figure 1 contains the records' notation.

[c]Start date is likely down biased because of midterm deviation at around 3100–3200 kyr (Figure 1).

[d]Strongly skewed error distribution occurs because of solution near interval bound.

[e]Error is not determined (likely > 50%).

[f]Weighted 50%-trimmed mean with maximum of internal and external $1 - \sigma$ error. Trimming [*Tukey*, 1977] ensured that biased or strongly skewed individual results were excluded from averaging. Degree of trimming has little influence on result.

[g]Internal error, superimposed is a timescale error of 25 kyr.

[h]External error.

parameters (start, end, amplitude). (3) Repeat steps 1 and 2 to produce 400 copies of simulated parameters. (4) Take standard deviation of each set of copies as uncertainty estimate.

[11] Comparing the mean of each set of copies with the original result showed that all estimations carried out had negligible bias. Because statistical uncertainties of start and end (Table 3) are clearly larger than timescale uncertainties (Table 2) the regressions do not require timescale simulations.

3.2. Calibration of $\delta^{18}O$ Changes

[12] Calibration formulas are required to calculate temperature or salinity changes into $\delta^{18}O$ changes, and vice versa. We used the calibration of temperature-related $\delta^{18}O$ changes from modern and experimental data [*Chen*, 1994], $\Delta\delta^{18}O_T/\Delta T = -0.234$‰/°C. An estimation of the statistical error ($1 - \sigma$) of this formula yields 0.003‰/°C, which we inflated in a conservative approach to a value of 0.01‰/°C (S. Mulitza, Research Center Ocean Margins, personal communication, 2004) to take "species noise" and violations of the actualism assumption into account. The calibration of salinity-related $\delta^{18}O$ changes, $\Delta\delta^{18}O_S/\Delta T = 0.05$‰/°C, assumes a linear relation between salinity and temperature changes and was developed for interpreting western equatorial Pacific $\delta^{18}O$ amplitudes [*Whitman and Berger*, 1992]. Systematic errors caused by applying the calibration to other sites are likely small owing to the low signal proportion of $\Delta\delta^{18}O_S$.

4. Results

4.1. NHG Start and End

[13] The results exhibit considerable variations in NHG start and end among the $\delta^{18}O$ records (Figures 1 and 2 and Table 3). The reason for this scatter is that the global ice volume signal of the NHG ($\delta^{18}O$ increase), common to all records owing to an ocean mixing time of less than ~2 kyr [*Broecker et al.*, 1988, 2004], is obscured by noise, mainly of climatic origin (regional temperature and salinity fluctuations). We assume that the variations in estimated start and end cancel out when averaging the results from many

records. This is a reasonable assumption, given climatological evidence for regional differences in temperature sensitivity [*Ravelo et al.*, 2004] and the fact that our NHG $\delta^{18}O$ database is so large. The average start and end values of the NHG ice volume increase are 3606 ± 60 kyr and 2384 ± 64 kyr, respectively, for the high-resolution records (Figure 1 and Table 3). The low-resolution records (Figure 2) yield an end date of 2510 ± 125 kyr that agrees within error bars, and a start date of 3350 ± 120 kyr that reflects minor systematic uncertainties. Sources of this error can be midterm deviations from the ramp form at around the start (see below) or underestimated influences of hiatuses in the low-resolution records.

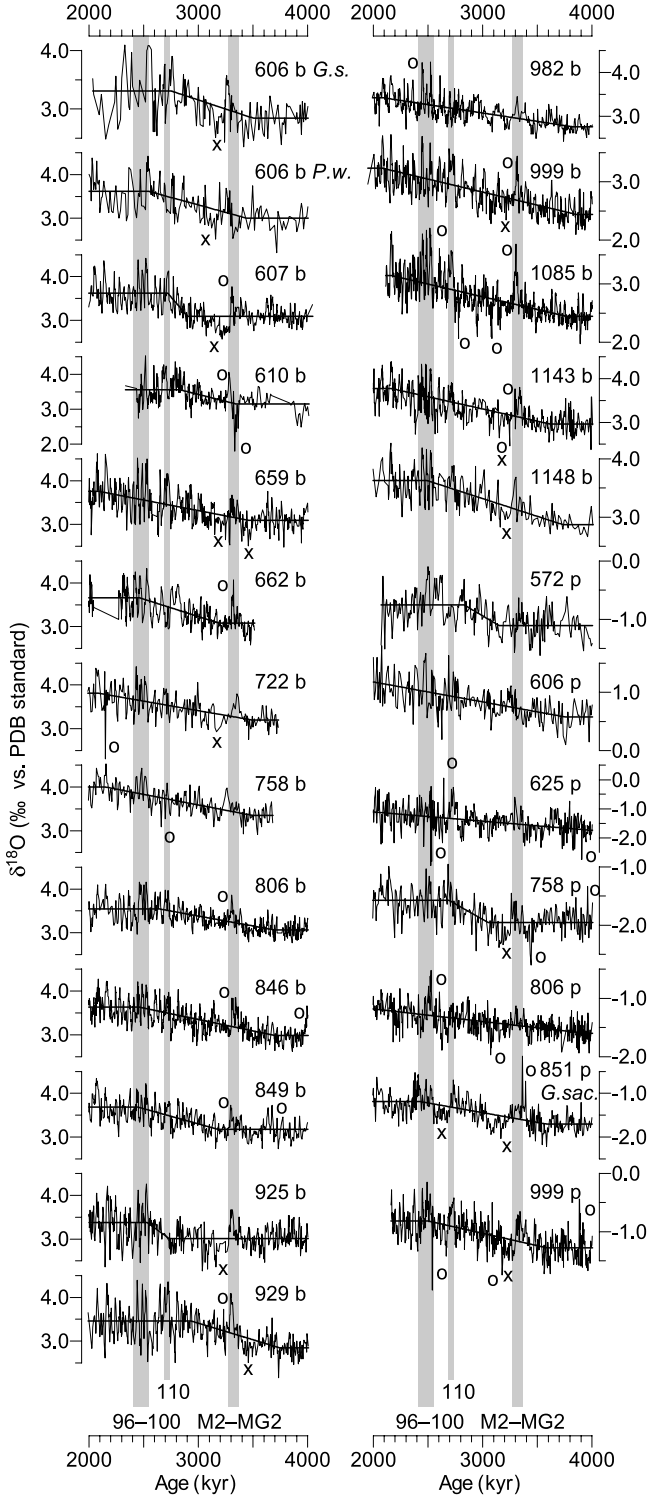

Figure 1. Determination of start, end, and $\delta^{18}O$ increase of the Northern Hemisphere glaciation (NHG), high-resolution records. The time series (light lines) were analyzed using ramp regression [*Mudelsee*, 2000] to determine long-term trend (bold lines). Regions of midterm systematic deviations from the trend are marked with crosses; regression outliers ($> 3\ \sigma(t)$) are marked with circles. Numbers refer to DSDP (572 to 610) and ODP (625 to 1148) sites; index "b" ("p") after site number refers to a benthic (planktonic) record. Abbreviations are *G.s.*, *G. subglobosa*; *G.sac.*, *G. sacculifer*; and *P.w.*, *P. wuellerstorfi.* Dates [*Lisiecki and Raymo*, 2005] of marine isotope stage (MIS) 96–100, 110, and M2–MG2 are widened (shaded) by ±25 kyr to account for timescale uncertainties. For results from low-resolution records, see Figure 2.

4.2. Ice Volume Signal

[14] Extraction of the NHG ice volume signal within the interval 2384 to 3606 kyr cannot be achieved by averaging results from individual records because the noise components temperature and salinity would not cancel out but reflect an overall cooling. Evaluating the size of the ice volume amplitude alone on the basis of the $\delta^{18}O$ results (Table 3) suggests an upper limit of around 0.4‰. This is indicated by values from records from several, low-latitude locations (925 b, 572 p, 625 p, 758 p, 806 p; see Figure 1 for notation), because a warming at all these sites across the NHG seems unlikely. More detailed information has to come from independent temperature proxy records from the same locations and water masses as the $\delta^{18}O$ records. The problem is that these temperature records are scarce, which is the reason why we used all available records (including those with a low time resolution). The SST record (cold and warm season averaged) from DSDP 572 [*Hays et al.*, 1989], based on ostracoda assemblages, shows a minimal cooling (Figure 3 and Table 3) during 2384–3606 kyr, equivalent to a $\delta^{18}O$ increase of $\Delta\delta^{18}O_T = 0.03 \pm 0.12$‰. Adopting the linear relation of *Whitman and Berger* [1992] between temperature and salinity changes, the cooling relates to a salinity-related $\delta^{18}O$ decrease, $\Delta\delta^{18}O_S = -0.01$‰. Subtracting $\Delta\delta^{18}O_T$ and $\Delta\delta^{18}O_S$ from the 572 p amplitude of 0.36 ± 0.06‰ yields an NHG ice volume signal of $\Delta\delta^{18}O_I = 0.34 \pm 0.13$‰. The high-resolution SST record from ODP 806 [*Andersson*, 1997], based on foraminifera assemblages, reveals a remarkable warming of 0.85 ± 0.17°C, equivalent to $\Delta\delta^{18}O_T = -0.20 \pm 0.04$‰ and $\Delta\delta^{18}O_S = 0.04$‰, converting the low 806 p amplitude (Table 3) into an ice volume signal of $\Delta\delta^{18}O_I = 0.43 \pm 0.06$‰. The BWT record from ODP 806 [*Lear et al.*, 2003], based on Mg/Ca thermometry, reveals despite its low resolution that, while

the surface waters warmed at the Ontong Java Plateau (western equatorial Pacific) across the NHG, the deep waters cooled ($\Delta\delta^{18}O_T$ = 0.24 ± 0.12‰, $\Delta\delta^{18}O_S$ = −0.05‰, and $\Delta\delta^{18}O_I$ = 0.25 ± 0.13‰). The Mg/Ca–derived BWT record from DSDP 607 [*Dwyer et al.*, 1995], has $\Delta\delta^{18}O_T$ = 0.15 ± 0.07‰, $\Delta\delta^{18}O_S$ = −0.03‰, and $\Delta\delta^{18}O_I$ = 0.41 ± 0.09‰. The Mg/Ca–derived BWT decrease of 1°C between 3.7 and 2.5 Ma (not continuously measured) at site ODP 1085 (D. H. Andreasen, Rutgers University, personal communication, 2004), finally, translates into $\Delta\delta^{18}O_I$ = 0.35‰. It is remarkable that the few Pliocene temperature records available so far, derived from distributed geographical sites and water masses with different proxy techniques, reveal, within error bars, the same ice volume signal of the NHG between 3606 and 2384 kyr, namely, an increase of $\Delta\delta^{18}O_I$ = 0.39 ± 0.04‰ (weighted mean). The equivalent sea level lowering [*Mix and Ruddiman*, 1984] is 43 m, with an uncertainty of somewhat more than 5 m.

4.3. Climate Variability

[15] The time-dependent $\delta^{18}O$ standard deviation, $\sigma(t)$, measuring the size of shorter-term fluctuations in ice volume, temperature, and salinity, shows an increase across the NHG, from 3200 kyr and ∼0.2‰ to 2560 kyr and ∼0.3‰ (Figure 4). No significant differences were found between benthic and planktonic records. A qualitatively similar long-term increase in variability had previously been recognized in the benthic $\delta^{18}O$ record from DSDP 552 [*Shackleton et al.*, 1988]. The timing and slowness of the increase in standard deviation support the timing and slowness of the increase in mean ice volume in the Northern Hemisphere: Ice sheets have to exist before fluctuations in their size occur.

4.4. Climate Persistence

[16] The estimated persistence time, τ, of $\delta^{18}O$ fluctuations is of the order of a few kiloyears (Table 3). Correlation analyses showed that τ does not depend on the sedimentation rate (Table 2; r = 0.06) or the temporal spacing (Table 2; r = −0.04), which means that the sampling or effects within the sediment cores such as bioturbation likely did not influence τ. Rather, the persistence is thought to be of climatic origin and reflect the time constant [*Imbrie and Imbrie*, 1980] of the fluctuating part of the Antarctic and the developing Arctic ice sheets. The values are slightly smaller for planktonic than for benthic records, which we explain by a stronger "dilution" of the planktonic signal by short-term atmospheric interactions of surface waters. The benthic τ estimates, averaging to 7.1 ± 0.4 kyr, should come closest to the time constant of Pliocene ice sheets. This value is significantly

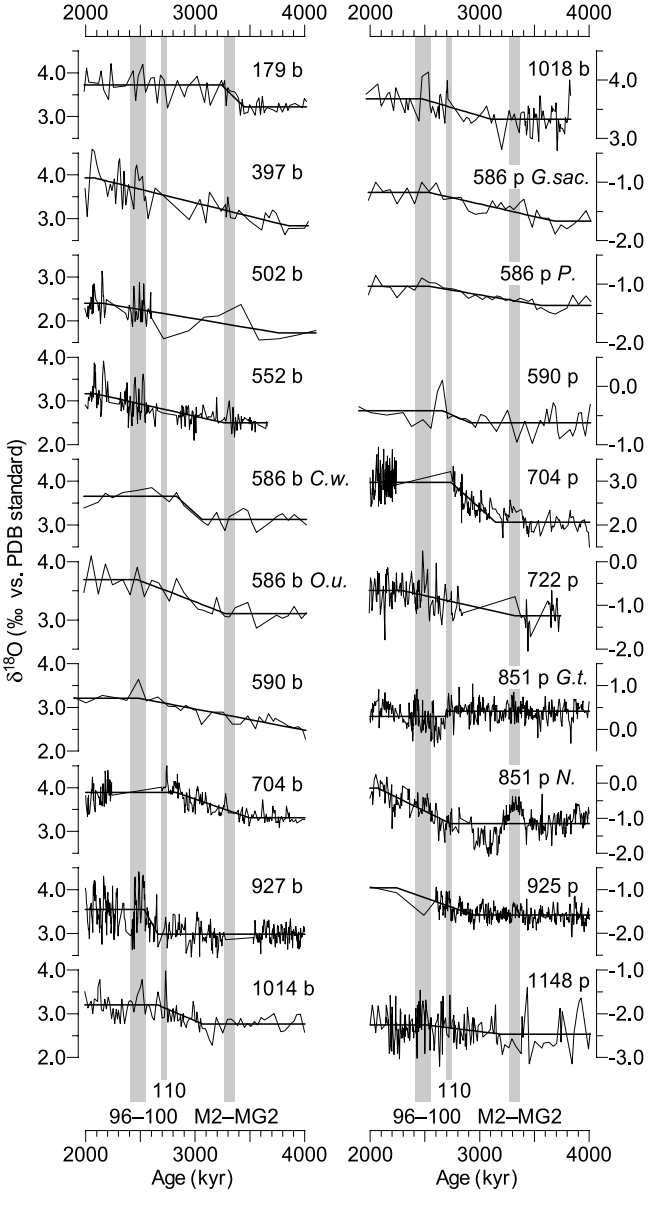

Figure 2. Determination of start, end, and $\delta^{18}O$ increase of the NHG, low-resolution records. Also included here are records with high time resolution but other defects (e.g., hiatuses) that presumably exclude an accurate estimation. Two benthic records (*C.w.*, *C. wuellerstorfi* and *O.u.*, *O. umbonatus*) and two planktonic records (*G.sac.*, *G. sacculifer* and *P.*, *Pulleniatina spp.*) are available from DSDP 586. Three high-resolution planktonic records are available from ODP 851. The first record (*G. sacculifer*) is shown in Figure 1. Both other records, shown here (*G.t.*, *G. tumida* and *N.*, *N. humerosa* and *N. dutertrei*), exhibit pronounced deviations in trend from the first record; 851 p *G.t.* thereby shows an unrealistic abrupt transition and is not considered further. *Cannariato and Ravelo* [1997] explain the low proportion of the ice volume signal in the latter two records. Average start of the $\delta^{18}O$ increase, calculated using the low-resolution records, is (weighted 50%-trimmed mean, with maximum of 1 − σ internal/external error and imposing a timescale uncertainty of 100 kyr) 3350 ± 120 kyr; average end is 2510 ± 125 kyr. Regions of midterm systematic deviations from the ramp form or regression outliers are not marked.

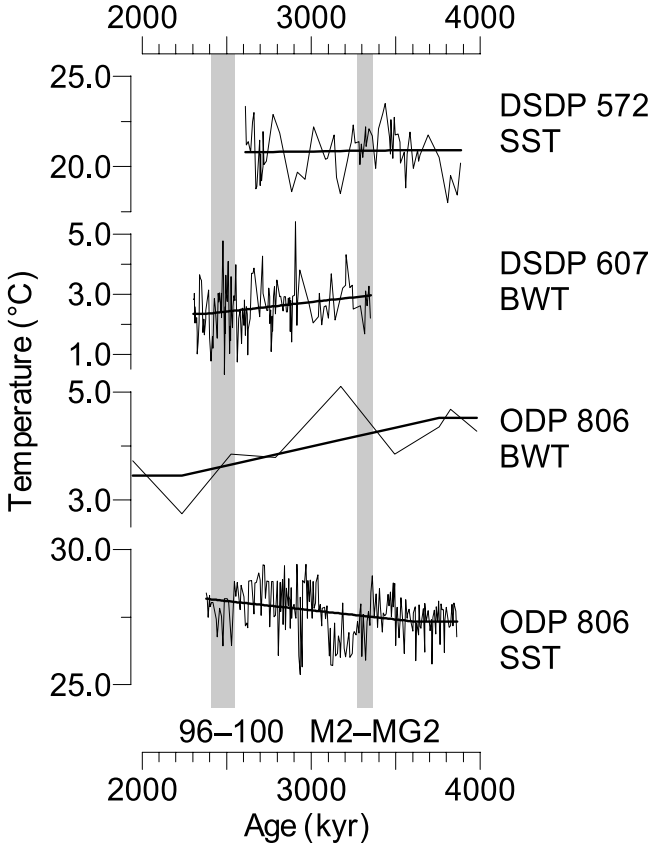

Figure 3. Determination of the temperature amplitude of the NHG between 3606 and 2384 kyr. SST is sea surface temperature; BWT is bottom water temperature. The amplitudes were determined using fitted ramps (bold lines) to the continuous data (light lines) with fixed start and end dates. Errors ($1 - \sigma$) were determined using computer simulations (section 3.1). The resulting temperature amplitudes are as follows (negative values indicate cooling): DSDP 572, SST of -0.12 ± 0.47°C; DSDP 607, BWT of -1.01 ± 0.51°C; ODP 806, BWT of -0.62 ± 0.29°C; and ODP 806, SST of $+0.85 \pm 0.17$°C.

smaller than the 17 kyr for the larger late Pleistocene ice sheets [*Imbrie and Imbrie*, 1980], in agreement with recent sedimentation modeling [*Lisiecki and Raymo*, 2005].

4.5. NHG Dynamics

[17] Over the 2–4 Myr interval, more or less all of the analyzed records (Figures 1, 2, and 3) exhibit a long-term trend, which is well described by the ramp model. There were few short excursions (extremes) and midterm deviations from this trend. The earliest $\delta^{18}O$ extreme of likely global significance within 2–4 Myr was at marine isotope stages (MIS) M2–MG2 (3295–3340 kyr [*Lisiecki and Raymo*, 2005]), detected in 11 of 25 high-resolution records as a glacial event exceeding three standard deviations (Figure 1). Stage M2 seems to reflect a stronger glaciation than stage MG2 [*Lisiecki and Raymo*, 2005]. The global

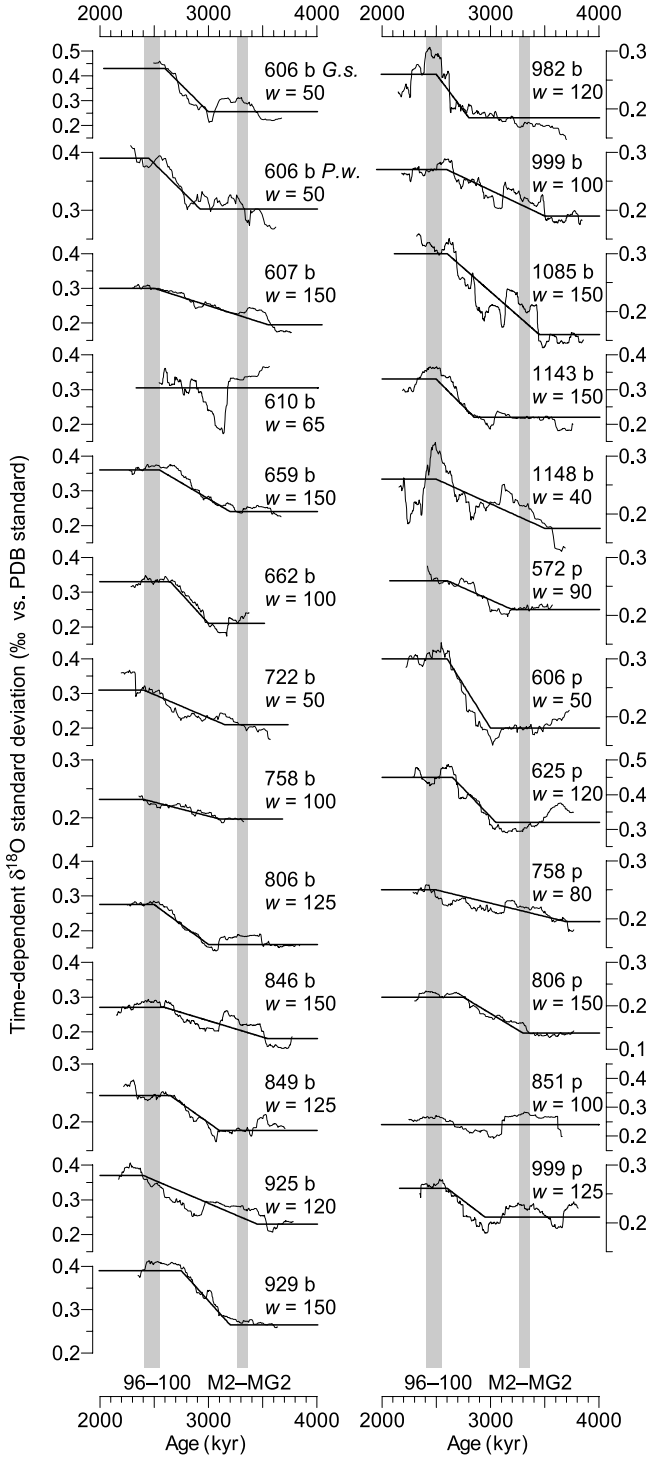

Figure 4. Determination of start, end, and increase of the time-dependent $\delta^{18}O$ standard deviation during the NHG, high-resolution records. Standard deviation (light lines) was estimated using detrended time series and a running window (w is the number of points). Best fit ramps (heavy lines) are also shown. Average start of the increase in standard deviation is 3200 kyr, average end is 2560 kyr, and average increase is by a factor of 1.5 (from ~0.2‰ to ~0.3‰).

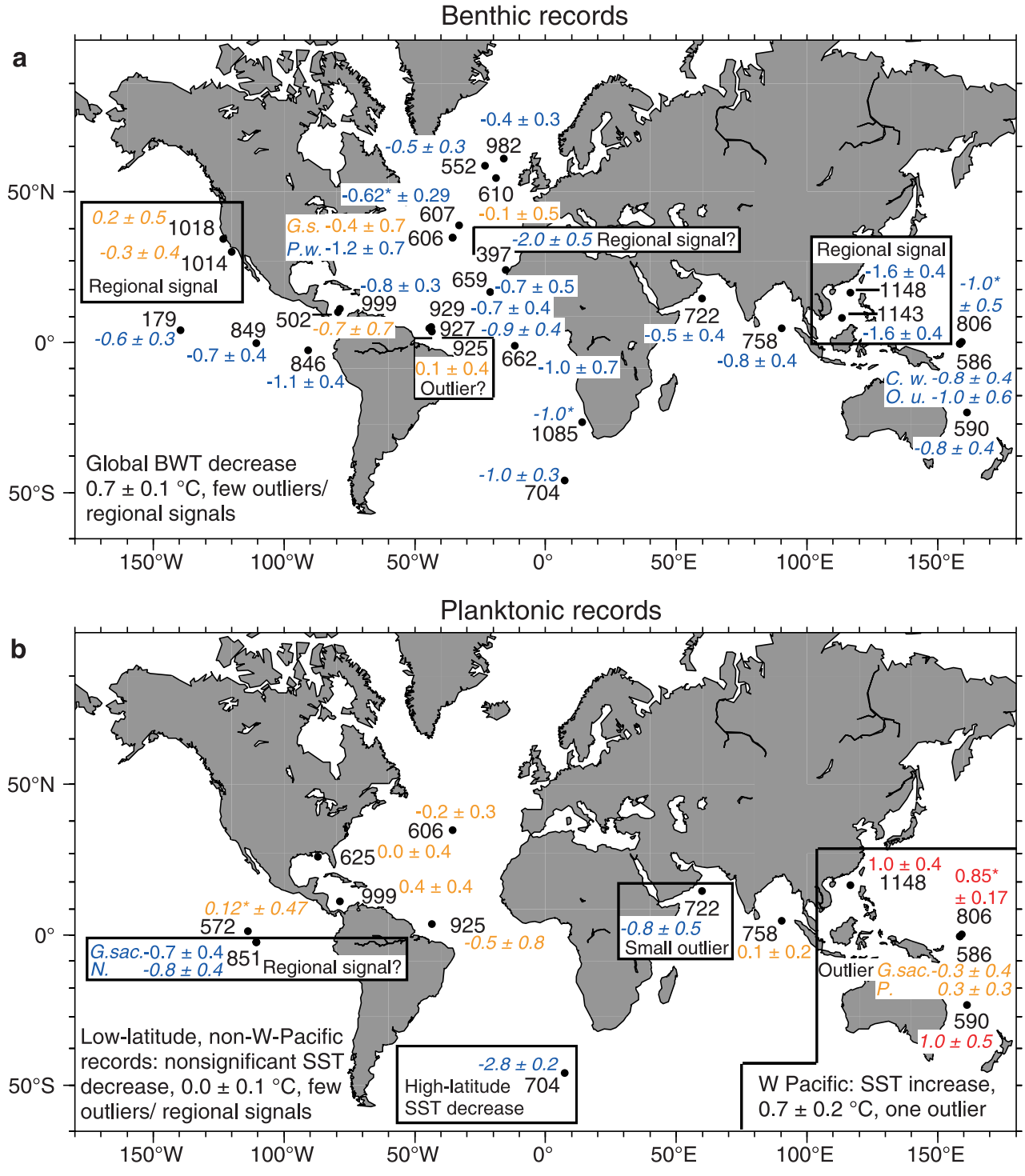

Figure 5. NHG temperature trends, all records. (a) Benthic and (b) planktonic data. Site locations are shown as dots; black numbers refer to DSDP (397 to 610) and ODP (625 to 1148) sites; black "179" refers to the V28-179 site. Temperature changes are in °C for the interval 3606 to 2384 kyr (high-resolution records, Table 1; low-resolution records, calculated from results (Figure 2) using calibrations (section 3.2)). Negative values indicate cooling; errors are 1 − σ. Significant cooling (warming) amplitudes are in blue (red), nonsignificant amplitudes are in orange; and values from high-resolution (low-resolution) records are in roman (italic) type. Five amplitudes (marked by asterisk) are from temperature proxy records (Figure 3). *C.w.*, *C. wuellerstorfi*; *G.s.*, *G. subglobosa*; *G.sac.*, *G. sacculifer*; *N.*, *N. humerosa* and *N. dutertrei*; *O.u.*, *O. umbonatus*; *P.*, *Pulleniatina* spp.; and *P.w.*, *P. wuellerstorfi.* Also shown in black boxes is a provisional spatial grouping of the different temperature changes.

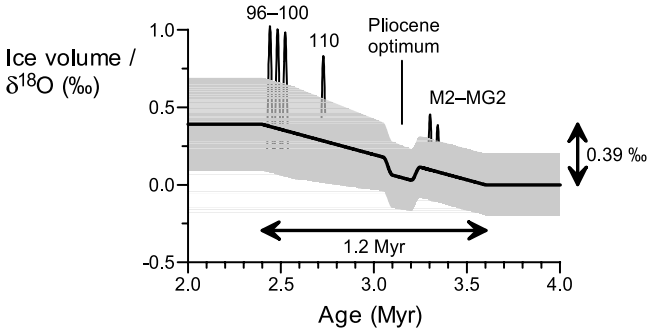

Figure 6. Schematic view of the NHG climate transition in the Pliocene. The mean ice volume (solid line) had a long-term increase from 3.6 to 2.4 Ma. The amplitude was 0.39‰ ($\delta^{18}O$ equivalent). The size of the $\delta^{18}O$ fluctuations around this trend (shaded band) increased slowly from 3.2 Myr and 0.2‰ to 2.56 Myr and 0.3‰. A midterm deviation from the glaciation trend was the Pliocene climate optimum from 3.25 Myr to 3.05 Myr. Short-term glaciations, perhaps driven by Earth's obliquity variations, occurred after the NHG start, at MIS MG2 (3.340 Ma) and M2 (3.295 Ma); the M2 glaciation was stronger than the MG2 glaciation. Further glaciations were at MIS 110 (2.7 Ma) and MIS 96, 98, and 100 (2.433–2.523 Myr). (Note that zero point of *y* axis is arbitrary.)

signature and IRD evidence from several sites in the North Atlantic/Nordic Seas [*Kleiven et al.*, 2002] indicate a significant northern ice volume proportion. A systematic, midterm deviation from the glaciation trend was the Pliocene climate optimum [*Dowsett et al.*, 1994], documented in 12 of 25 globally distributed, high-resolution records as an interval of lowered $\delta^{18}O$ from ~3250 kyr to ~3050 kyr (Figure 1). Given the duration and the size of the $\delta^{18}O$ decrease in many records (e.g., 607 b), a significant deglaciation seems likely. As regards the dispute about the stability of the Pliocene Antarctic ice shield [*Shackleton et al.*, 1995a], our results combined with the IRD evidence [*Kleiven et al.*, 2002] suggest that this deglaciation could have been a Northern Hemisphere event, leaving the Antarctic shield intact. Other, more heterogeneously distributed, shorter-term cold and warm extremes accompanied the long-term NHG glaciation trend (Figure 1) until a critical threshold was passed at 2.7 Ma [*Haug et al.*, 1999] and strong glaciations (often exceeding 3 σ in Figure 1) at MIS 96–98–100 (2433–2523 kyr [*Lisiecki and Raymo*, 2005]) occurred. This heterogeneity and the above finding of spatial variations in start, end, and $\delta^{18}O$ amplitude indicate differences on short-term to midterm timescales (~41–100 kyr) among regional temperature histories across the NHG (Table 3). This supports the idea that during a global climate change, regional subsystems with varying feedback mechanisms emerge in response [*Ravelo et al.*, 2004].

[18] In the geographical distribution of the long-term NHG temperature change (Figure 5), we see following provisional grouping. Bottom water cooling was, within the error ranges, more or less globally homogenous. Only 6 of 29 benthic records reflect larger deviations (Figure 5a), which may be due to reduced data quality (low-resolution records) or regional influences such as changes in upwelling (e.g., at DSDP 397 site). It is unclear why the result from the benthic record at site ODP 925 (0.1°C warming) deviates significantly from the results from nearby sites ODP 927 (0.9°C cooling) and ODP 929 (0.7°C cooling). The remaining 23 records have an average BWT decrease of ~0.7°C.

[19] SST changes (Figure 5b) are divided into three groups. First, high latitudes likely cooled strongly (704 p). Second, at lower latitudes, the surface waters in the western Pacific region warmed significantly, by ~0.7°C on average. Third, low-latitude surface waters elsewhere had, to first order, no long-term temperature change, which supports to some degree the hypothesis of a temperature buffer [*Jenkins*, 1992]. However, this does not apply to the western Pacific (warming) or some other regions (e.g., Sites 851 and 722). A more detailed picture of NHG temperature trends will emerge when more high-resolution BWT and SST records for the 2–4 Myr interval become available.

5. Conclusions

[20] The schematic view of the NHG (Figure 6) underlines that this climate transition was gradual. The amplitude of the change in mean ice volume (0.39‰) is only one to two times stronger than the average noise level, and is up to two times weaker than the largest glacial $\delta^{18}O$ excursions (~0.8‰) from the long-term trend (Figures 1 and 2). (The low signal-to-noise ratio of the climate transition is an a posteriori confirmation of our approach to construct and analyze a large database.) The timing of the change in mean ice volume (from 3.6 to 2.4 Ma) allows us to evaluate the feasibility of causal explanations of the NHG.

[21] A recent paper [*Knie et al.*, 2004] proposed that a supernova explosion occurred close to the solar system, at 2.8 Ma, based on iron isotope data in a manganese crust. This could have led to an enhanced cosmic ray flux for a few 100 kyr. It was cautiously suggested that, provided there is a negative correlation between cosmic ray flux and Earth's surface temperature, "this supernova could have triggered a climatic change" [*Knie et al.*, 2004, p. 171103-3], that is, the NHG. In light of our finding that the NHG began at 3.6 Ma, the supernova explanation becomes unlikely.

[22] *Willis et al.* [1999] noted spectral power at periods less than or equal to 15 kyr in a climate record based on pollen data from the Pula maar, Hungary, which spans the interval between 3.05 and 2.6 Ma. *Willis et al.* [1999, p. 571] proposed that "a nonlinear response at sub-Milankovitch frequencies may have been responsible for the initiation of the NHG." The early start of the NHG at 3.6 Ma (Figure 6) again does not support this view. Other attempts to relate the initiation of the NHG to changes in spectral power are also not compatible with the early cooling trend documented here. For example, *Maslin et al.* [1998] proposed that an increase in obliquity minima from 3.2 to 2.5 Ma may have triggered the NHG. We do not dispute that Milankovitch variability may have influenced Pliocene to Pleistocene climate evolution; however, we do not believe such variability was the trigger for the NHG. The initiation of

NHG was a long-term climate change, affecting such important variables as ice volume and temperature, and numerous feedback effects likely occurred from 3.6 to 2.4 Myr ago.

[23] The slow ice buildup (Figure 6) indicates a slow, tectonic mechanism as the probable root cause of NHG. The shoaling of the Central American Seaway in the Pliocene was suggested by *Keigwin* [1982a]. This tectonic movement led to a restricted water mass exchange between the Atlantic and the Pacific Oceans and to an intensified Gulf Stream, which brought moisture to high northern latitudes [*Keigwin*, 1982a]. However, a comparison of Atlantic/Pacific records of neodymium and lead isotopes [*Frank et al.*, 1999] revealed that the restriction in water mass exchange was essentially complete by 5 Ma. Although the present study sets the NHG start earlier than previous work, we think that the disagreement in timing is still a strong argument against invoking the shoaling of the Central American Seaway as the explanation of NHG. Furthermore, two modeling studies [*Nisancioglu et al.*, 2003; *Klocker et al.*, 2005] show that an enhanced northward moisture transport is accompanied by enhanced heat transport, which can delay the start of a glaciation as originally proposed by *Berger and Wefer* [1996].

[24] Another tectonic mechanism is Tibetan uplift, proposed to have led to weathering-induced atmospheric carbon dioxide removal [*Raymo et al.*, 1988]. Here the precise timing of when this movement became climatologically effective is not accurately constrained and might have been well before the NHG start [*Raymo and Ruddiman*, 1992; *Molnar et al.*, 1993; *Spicer et al.*, 2003]. Carbon dioxide proxy records are also needed to test this hypothesis directly. Currently available records employ the stomata index in oaks [*Kürschner et al.*, 1996], or boron and carbon isotopes in marine matter [*Raymo et al.*, 1996; *Pagani et al.*, 1999; *Pearson and Palmer*, 2000]. These records suggest that Miocene-Pliocene carbon dioxide concentrations were not doubled but were possibly 30% higher than preindustrial levels. This evidence is not sufficient to accept or reject the Tibetan uplift hypothesis.

[25] Tibetan uplift could also have resulted in other important changes to the climate system. For instance, a sudden, tenfold increase in atmospheric dust load at 3.6 Ma has been related to aridification due to Tibetan uplift [*Rea et al.*, 1998]. This increase, in good agreement with the NHG start, could have been responsible for the cooling that permitted increased snow and ice buildup on Northern Hemisphere land surfaces [*Rea et al.*, 1998]. A strengthening of the east Asian monsoon from 3.6 to 2.6 Ma [*Zhisheng et al.*, 2001] could also have strengthened the weathering process. The above dates correspond with the inferred NHG initiation (Figure 6) and suggest Tibetan uplift may have affected global climate evolution at this time.

[26] A final tectonic mechanism that fits our derived NHG time frame is the proposed restriction of the Indonesian Seaway between 4 and 3 Myr ago [*Cane and Molnar*, 2001]. This event could have reduced the atmospheric heat transport from the tropics to higher northern latitudes in the Pacific region. It could also explain the observed NHG warming of surface waters in the western Pacific region (Figure 5b) by the accumulation of westward flowing, equatorial surface waters.

[27] Two major causes for explaining the Pliocene warmth interval (3.25 to 3.05 Ma) have been brought forward. The first, elevated atmospheric CO_2 levels, is problematic because it is not well corroborated by data [see also *Crowley*, 1996]. Elevated CO_2 is also difficult to reconcile with the Tibetan uplift NHG explanation. The required positive, $\sim$200-kyr-long CO_2 deviation from a long-term downward trend could have come from a variation in terrestrial plant biomass, as was suggested for the late Pleistocene glacial-interglacial cycle [e.g., *Shackleton*, 1977]. If so, one should search for evidence for significant Pliocene biomass changes. These could be a consequence of the NHG initiation. The second cause, stronger oceanic heat transport, is not feasible to explain a global warming event because, to first order, it merely redistributes heat on the planet [*Crowley*, 1996]. Since the results of the PRISM group [*Dowsett et al.*, 1994, 2005] show that the Pliocene climate optimum occurred at a wide spatial scale, this explanation is thus problematic. However, surface waters at site ODP 806 in the western equatorial Pacific exhibit a pronounced cooling during the Pliocene warmth (Figure 3). This can be interpreted as heat that was transported steadily away from that region. Transport direction was predominantly northward. This heat may have melted parts of the newly built up Northern Hemisphere ice sheets (see section 4.5 and *Haywood and Valdes* [2004]). The ice-albedo feedback would have enhanced this midterm Pliocene warming signal [*Haywood and Valdes*, 2004]. Another transport mechanism could have been enhanced heat transport by winds. Long-term changes in wind properties can be induced by orographic changes. The feasibility of such scenarios in context of the NHG and the Pliocene warmth could be analyzed using coupled global climate models (GCMs). For example, *Chandler et al.* [1994], *Sloan et al.* [1996], and *Haywood and Valdes* [2004] studied the middle Pliocene climate using GCMs.

[28] The long-term glaciation trend of the Northern Hemisphere eventually led to thresholds in the climate system being exceeded and thereby shorter-term, positive feedback mechanisms initiated. Such feedbacks could have been a shift toward stratification in the polar ocean at 2.7 Myr ago, which may have trapped additional carbon dioxide in the abyss [*Haug et al.*, 1999; *Sigman et al.*, 2004] and also provided moisture to northern North America [*Haug et al.*, 2005]. The strong glaciation at MIS 110 [*Haug et al.*, 1999] would have been a consequence of this amplification of the long-term glaciation trend. The climate system finally came into a new, quasi-stable state with Milankovitch-type glacial-interglacial cycles [*Berger et al.*, 1984], which have persisted to the present.

[29] **Acknowledgments.** We gratefully acknowledge the remarks by an anonymous reviewer and the Editor, L. Sloan. We thank C. Andersson, D. Andreasen, W. Berger, T. Bickert, K. Billups, J. Chen, S. Clemens, W. Curry, J. Farrell, G. Haug, Z. Jian, L. Lisiecki, A. Mix, D. Oppo, W. Prell, A. Ravelo, R. Tiedemann, and the ODP data librarian for the release of published and unpublished data and S. Cande, B. Clement, G. Haug, S. Mulitza, D. Schrag, and M. Schulz for comments. Supported by DFG research grant MU 1595/2 (M.M.).

References

Andersson, C. (1997), Transfer function vs. modern analog technique for estimating Pliocene sea-surface temperatures based on planktic foraminiferal data, western equatorial Pacific Ocean, *J. Foraminiferal Res.*, *27*, 123–132.

Andreasen, D. H. (2001), Isolating sources of Plio-Pleistocene paleoclimate variability, Ph. D. dissertation, 236 pp., Univ. of Calif., Santa Cruz.

Baksi, A. K., V. Hsu, M. O. McWilliams, and E. Farrar (1992), $^{40}Ar/^{39}Ar$ dating of the Brunhes-Matuyama geomagnetic field reversal, *Science*, *256*, 356–357.

Baksi, A. K., K. A. Hoffman, and M. McWilliams (1993), Testing the accuracy of the geomagnetic polarity time-scale (GPTS) at 2–5 Ma, utilizing $^{40}Ar/^{39}Ar$ incremental heating data on whole-rock basalts, *Earth Planet. Sci. Lett.*, *118*, 135–144.

Berger, A., J. Imbrie, J. Hays, G. Kukla, and B. Saltzman (Eds.) (1984), *Milankovitch and Climate*, 895 pp., Springer, New York.

Berger, W. H., and G. Wefer (1996), Expedition into the past: Paleoceanographic studies in the South Atlantic, in *The South Atlantic: Present and Past Circulation*, edited by G. Wefer et al., pp. 363–410, Springer, New York.

Berggren, W. A., F. J. Hilgen, C. G. Langereis, D. V. Kent, J. D. Obradovich, I. Raffi, M. E. Raymo, and N. J. Shackleton (1995), Late Neogene chronology: New perspectives in high-resolution stratigraphy, *Geol. Soc. Am. Bull.*, *107*, 1272–1287.

Bickert, T., W. B. Curry, and G. Wefer (1997), Late Pliocene to Holocene (2.6–0 Ma) western equatorial Atlantic deep-water circulation: Inferences from benthic stable isotopes, *Proc. Ocean Drill. Program Sci. Results*, *154*, 239–254.

Billups, K., A. C. Ravelo, and J. C. Zachos (1998a), Early Pliocene deep water circulation in the western equatorial Atlantic: Implications for high-latitude climate change, *Paleoceanography*, *13*, 84–95.

Billups, K., A. C. Ravelo, and J. C. Zachos (1998b), Early Pliocene climate: A perspective from the western equatorial Atlantic warm pool, *Paleoceanography*, *13*, 459–470.

Broecker, W. S., M. Andree, G. Bonani, W. Wolfli, H. Oeschger, M. Klas, A. Mix, and W. Curry (1988), Preliminary estimates for the radiocarbon age of deep water in the glacial ocean, *Paleoceanography*, *3*, 659–669.

Broecker, W. S., E. Clark, I. Hajdas, and G. Bonani (2004), Glacial ventilation rates for the deep Pacific Ocean, *Paleoceanography*, *19*, PA2002, doi: 10.1029/2003PA000974.

Cande, S. C., and D. V. Kent (1992), A new geomagnetic polarity time scale for the late Cretaceous and Cenozoic, *J. Geophys. Res.*, *97*, 13,917–13,951.

Cane, M. A., and P. Molnar (2001), Closing of the Indonesian seaway as a precursor to east African aridification around 3–4 million years ago, *Nature*, *411*, 157–162.

Cannariato, K. G., and A. C. Ravelo (1997), Pliocene-Pleistocene evolution of eastern tropical Pacific surface water circulation and thermocline depth, *Paleoceanography*, *12*, 805–820.

Chaisson, W. P., and A. C. Ravelo (1997), Changes in upper water-column structure at Site 925, late Miocene–Pleistocene: Planktonic foraminifer assemblage and isotopic evidence, *Proc. Ocean Drill. Program Sci. Results*, *154*, 255–268.

Chandler, M., D. Rind, and R. Thompson (1994), Joint investigations of the middle Pliocene climate II: GISS GCM Northern Hemisphere results, *Global Planet. Change*, *9*, 197–219.

Chen, J. (1994), Benthic foraminiferal isotope composition: Implications for late Neogene–Quaternary paleoceanography of the Indian Ocean, Ph. D. dissertation, 492 pp., Brown Univ., Providence, R. I.

Chen, J., J. W. Farrell, D. W. Murray, and W. L. Prell (1995), Timescale and paleoceanographic implications of a 3.6 m.y. oxygen isotope record from the northeast Indian Ocean (Ocean Drilling Program Site 758), *Paleoceanography*, *10*, 21–47.

Clemens, S. C., D. W. Murray, and W. L. Prell (1996), Nonstationary phase of the Plio-Pleistocene Asian monsoon, *Science*, *274*, 943–948.

Clement, B. M., C. C. Swisher, and P. Rodda (1997), New magnetostratigraphic and $^{40}Ar/^{39}Ar$ dating results from the Suva Marl, Fiji: Calibration of the early Pliocene geomagnetic polarity time scale, *Earth Planet. Sci. Lett.*, *151*, 107–115.

Crowley, T. J. (1991), Modeling Pliocene warmth, *Quat. Sci. Rev.*, *10*, 275–282.

Crowley, T. J. (1996), Pliocene climates: The nature of the problem, *Mar. Micropaleontol.*, *27*, 3–12.

Curry, W. B., and K. G. Miller (1989), Oxygen and carbon isotopic variation in Pliocene benthic foraminifers of the equatorial Atlantic, *Proc. Ocean Drill. Program Sci. Results*, *108*, 157–166.

Dowsett, H., R. Thompson, J. Barron, T. Cronin, F. Fleming, S. Ishman, R. Poore, D. Willard, and T. Holtz Jr. (1994), Joint investigations of the middle Pliocene climate I: PRISM paleoenvironmental reconstructions, *Global Planet. Change*, *9*, 169–195.

Dowsett, H. J., M. A. Chandler, T. M. Cronin, and G. S. Dwyer (2005), Middle Pliocene sea surface temperature variability, *Paleoceanography*, *20*, PA2014, doi: 10.1029/2005PA001133.

Dwyer, G. S., T. M. Cronin, P. A. Baker, M. E. Raymo, J. S. Buzas, and T. Corrège (1995), North Atlantic deepwater temperature change during late Pliocene and late Quaternary climatic cycles, *Science*, *270*, 1347–1351.

Efron, B., and R. J. Tibshirani (1993), *An Introduction to the Bootstrap*, 436 pp., CRC Press, Boca Raton, Fla.

Elmstrom, K. M., and J. P. Kennett (1986), Late Neogene paleoceanographic evolution of Site 590: Southwest Pacific, *Initial Rep. Deep Sea Drill. Proj.*, *90*, 1361–1381.

Farrell, J. W., and T. R. Janecek (1991), Late Neogene paleoceanography and paleoclimatology of the northeast Indian Ocean (Site 758), *Proc. Ocean Drill. Program Sci. Results*, *121*, 297–355.

Frank, M., B. C. Reynolds, and R. K. O'Nions (1999), Nd and Pb isotopes in Atlantic and Pacific water masses before and after closure of the Panama gateway, *Geology*, *27*, 1147–1150.

Franz, S.-O. (1999), Pliozäne Zeitreihen zur Rekonstruktion der Tiefenwasserzirkulation und der siliziklastischen Amazonasfracht im äquatorialen Westatlantik (Ceara Schwelle, ODP Leg 154), *Rep. 84*, 183 pp., GEOMAR, Kiel, Germany.

Hall, C. M., and J. W. Farrell (1995), Laser $^{40}Ar/^{39}Ar$ ages of tephra from Indian Ocean deep-sea sediments: Tie points for the astronomical and geomagnetic polarity time scales, *Earth Planet. Sci. Lett.*, *133*, 327–338.

Haug, G. H., and R. Tiedemann (1998), Effect of the formation of the Isthmus of Panama on Atlantic Ocean thermohaline circulation, *Nature*, *393*, 673–676.

Haug, G. H., D. M. Sigman, R. Tiedemann, T. F. Pedersen, and M. Sarnthein (1999), Onset of permanent stratification in the subarctic Pacific Ocean, *Nature*, *401*, 779–782.

Haug, G. H., R. Tiedemann, R. Zahn, and A. C. Ravelo (2001), Role of Panama uplift on oceanic freshwater balance, *Geology*, *29*, 207–210.

Haug, G. H., et al. (2005), North Pacific seasonality and the glaciation of North America 2.7 million years ago, *Nature*, *433*, 821–825.

Hays, P. E., N. G. Pisias, and A. K. Roelofs (1989), Paleoceanography of the eastern equatorial Pacific during the Pliocene: A high-resolution radiolarian study, *Paleoceanography*, *4*, 57–73.

Haywood, A. M., and P. J. Valdes (2004), Modelling Pliocene warmth: Contribution of atmosphere, oceans and cryosphere, *Earth Planet. Sci. Lett.*, *218*, 363–377.

Hodell, D. A., and K. Venz (1992), Toward a high-resolution stable isotopic record of the Southern Ocean during the Pliocene-Pleistocene (4.8 to 0.8 Ma), in *The Antarctic Paleoenvironment: A Perspective on Global Change*, *Part One*, *Antarct. Res. Ser.*, vol. 56, edited by J. P. Kennett and D. A. Warnke, pp. 265–310, AGU, Washington, D. C.

Imbrie, J., and J. Z. Imbrie (1980), Modeling the climatic response to orbital variations, *Science*, *207*, 943–953.

Jansen, E., J. Sjøholm, U. Bleil, and J. A. Erichsen (1990), Neogene and Pleistocene glaciations in the Northern Hemisphere and late Miocene–Pliocene global ice volume fluctuations: Evidence from the Norwegian Sea, in *Geological History of the Polar Oceans: Arctic versus Antarctic*, edited by U. Bleil and J. Thiede, pp. 677–705, Springer, New York.

Jansen, E., L. A. Mayer, J. Backman, R. M. Leckie, and T. Takayama (1993), Evolution of Pliocene climate cyclicity at hole 806B (5–2 Ma): Oxygen isotope record, *Proc. Ocean Drill. Program Sci. Results*, *130*, 349–362.

Jenkins, D. G. (1992), Predicting extinctions of some extant planktic foraminifera, *Mar. Micropaleontol.*, *19*, 239–243.

Jian, Z., Q. Zhao, X. Cheng, J. Wang, P. Wang, and X. Su (2003), Plio-Pleistocene stable isotope and paleoceanographic changes in the northern South China Sea, *Palaeogeogr. Palaeoclimatol. Palaeoecol.*, *193*, 425–442.

Joyce, J. E., L. R. C. Tjalsma, and J. M. Prutzman (1990), High-resolution planktic stable isotope record and spectral analysis for the last 5.35 m.y.: Ocean Drilling Program Site 625 northeast Gulf of Mexico, *Paleoceanography*, *5*, 507–529.

Keigwin, L. (1982a), Isotopic paleoceanography of the Caribbean and east Pacific: Role of Panama uplift in late Neogene time, *Science*, *217*, 350–353.

Keigwin, L. D. Jr. (1982b), Stable isotope stratigraphy and paleoceanography of sites 502 and 503, *Initial Rep. Deep Sea Drill. Proj.*, *68*, 445–453.

Keigwin, L. D. (1986), Pliocene stable-isotope record of Deep Sea Drilling Project Site 606:

Sequential events of ^{18}O enrichment beginning at 3.1 Ma, *Initial Rep. Deep Sea Drill. Proj.*, *94*, 911–920.

Kleiven, H. F., E. Jansen, T. Fronval, and T. M. Smith (2002), Intensification of Northern Hemisphere glaciations in the circum Atlantic region (3.5–2.4 Ma)—Ice rafted detritus evidence, *Palaeogeogr. Palaeoclimatol. Palaeoecol.*, *184*, 213–223.

Klocker, A., M. Prange, and M. Schulz (2005), Testing the influence of the Central American Seaway on orbitally forced Northern Hemisphere glaciation, *Geophys. Res. Lett.*, *32*, L03703, doi: 10.1029/2004GL021564.

Knie, K., G. Korschinek, T. Faestermann, E. A. Dorfi, G. Rugel, and A. Wallner (2004), ^{60}Fe anomaly in a deep-sea manganese crust and implications for a nearby supernova source, *Phys. Rev. Lett.*, *93*(17), 171103, doi: 10.1103/PhysRevLett.93.171103.

Kürschner, W. M., J. van der Burgh, H. Visscher, and D. L. Dilcher (1996), Oak leaves as biosensors of late Neogene and early Pleistocene paleoatmospheric CO_2 concentrations, *Mar. Micropaleontol.*, *27*, 299–312.

Kwiek, P. B., and A. C. Ravelo (1999), Pacific Ocean intermediate and deep water circulation during the Pliocene, *Palaeogeogr. Palaeoclimatol. Palaeoecol.*, *154*, 191–217.

Larsen, H. C., A. D. Saunders, P. D. Clift, J. Beget, W. Wei, and S. Spezzaferri (1994), Seven million years of glaciation in Greenland, *Science*, *264*, 952–955.

Lear, C. H., Y. Rosenthal, and J. D. Wright (2003), The closing of a seaway: Ocean water masses and global climate change, *Earth Planet. Sci. Lett.*, *210*, 425–436.

Lisiecki, L. E., and M. E. Raymo (2005), A Plio-Pleistocene stack of 57 globally distributed benthic $\delta^{18}O$ records, *Paleoceanography*, *20*, PA1003, doi: 10.1029/2004PA001071.

Lyle, M., I. Koizumi, M. L. Delaney, and J. A. Barron (2000), Sedimentary record of the California Current system, middle Miocene to Holocene: A synthesis of Leg 167 results, *Proc. Ocean Drill. Program Sci. Results*, *167*, 341–376.

Maslin, M. A., X. S. Li, M.-F. Loutre, and A. Berger (1998), The contribution of orbital forcing to the progressive intensification of Northern Hemisphere glaciation, *Quat. Sci. Rev.*, *17*, 411–426.

Mix, A. C., and W. F. Ruddiman (1984), Oxygen-isotope analyses and Pleistocene ice volumes, *Quat. Res.*, *21*, 1–20.

Mix, A. C., N. G. Pisias, W. Rugh, J. Wilson, A. Morey, and T. K. Hagelberg (1995), Benthic foraminifer stable isotope record from Site 849 (0–5 Ma): Local and global climate changes, *Proc. Ocean Drill. Program Sci. Results*, *138*, 371–412.

Molnar, P., P. England, and J. Martinod (1993), Mantle dynamics, uplift of the Tibetan Plateau, and the Indian monsoon, *Rev. Geophys.*, *31*, 357–396.

Mudelsee, M. (2000), Ramp function regression: A tool for quantifying climate transitions, *Comput. Geosci.*, *26*, 293–307.

Mudelsee, M. (2002), TAUEST: A computer program for estimating persistence in unevenly spaced weather/climate time series, *Comput. Geosci.*, *28*, 69–72.

Mudelsee, M. (2005), A new, absolutely dated geomagnetic polarity timescale for the late Pliocene to early Pleistocene, in *Milutin Milankovitch 125th Anniversary Symposium: Paleoclimate and the Earth Climate System*, edited by A. Berger, M. Ercegovac, and F. Mesinger, Serb. Acad. of Sci. and Arts, Belgrade, in press.

Nisancioglu, K. H., M. E. Raymo, and P. H. Stone (2003), Reorganization of Miocene deep water circulation in response to the shoaling of the Central American Seaway, *Paleoceanography*, *18*(1), 1006, doi: 10.1029/2002PA000767.

Oppo, D. W., M. E. Raymo, G. P. Lohmann, A. C. Mix, J. D. Wright, and W. L. Prell (1995), A $\delta^{13}C$ record of upper North Atlantic deep water during the past 2.6 million years, *Paleoceanography*, *10*, 373–394.

Pagani, M., M. A. Arthur, and K. H. Freeman (1999), Miocene evolution of atmospheric carbon dioxide, *Paleoceanography*, *14*, 273–292.

Pearson, P. N., and M. R. Palmer (2000), Atmospheric carbon dioxide concentrations over the past 60 million years, *Nature*, *406*, 695–699.

Prell, W. L. (1985), Pliocene stable isotope and carbonate stratigraphy (holes 572C and 573A): Paleoceanographic data bearing on the question of Pliocene glaciation, *Initial Rep. Deep Sea Drill. Proj.*, *85*, 723–734.

Ravelo, A. C., D. H. Andreasen, M. Lyle, A. Olivarez Lyle, and M. W. Wara (2004), Regional climate shifts caused by gradual global cooling in the Pliocene epoch, *Nature*, *429*, 263–267.

Raymo, M. E. (1992), Global climate change: A three million year perspective, in *Start of a Glacial*, edited by G. J. Kukla and E. Went, pp. 207–223, Springer, New York.

Raymo, M. E. (1994), The initiation of Northern Hemisphere glaciation, *Annu. Rev. Earth Planet. Sci.*, *22*, 353–383.

Raymo, M. E., and W. F. Ruddiman (1992), Tectonic forcing of late Cenozoic climate, *Nature*, *359*, 117–122.

Raymo, M. E., W. F. Ruddiman, and P. N. Froelich (1988), Influence of late Cenozoic mountain building on ocean geochemical cycles, *Geology*, *16*, 649–653.

Raymo, M. E., W. F. Ruddiman, J. Backman, B. M. Clement, and D. G. Martinson (1989), Late Pliocene variation in Northern Hemisphere ice sheets and North Atlantic deep water circulation, *Paleoceanography*, *4*, 413–446.

Raymo, M. E., D. Hodell, and E. Jansen (1992), Response of deep ocean circulation to initiation of Northern Hemisphere glaciation (3–2 Ma), *Paleoceanography*, *7*, 645–672.

Raymo, M. E., B. Grant, M. Horowitz, and G. H. Rau (1996), Mid-Pliocene warmth: Stronger greenhouse and stronger conveyor, *Mar. Micropaleontol.*, *27*, 313–326.

Rea, D. K., H. Snoeckx, and L. H. Joseph (1998), Late Cenozoic eolian deposition in the North Pacific: Asian drying, Tibetan uplift, and cooling of the Northern Hemisphere, *Paleoceanography*, *13*, 215–224.

Renne, P., R. Walter, K. Verosub, M. Sweitzer, and J. Aronson (1993), New data from Hadar (Ethiopia) support orbitally tuned time scale to 3.3 Ma, *Geophys. Res. Lett.*, *20*, 1067–1070.

Shackleton, N. (1967), Oxygen isotope analyses and Pleistocene temperatures re-assessed, *Nature*, *215*, 15–17.

Shackleton, N. J. (1977), Carbon-13 in *Uvigerina*: Tropical rainforest history and the equatorial Pacific carbonate dissolution cycles, in *The Fate of Fossil Fuel CO_2 in the Oceans*, edited by N. R. Andersen and A. Malahoff, pp. 401–427, Springer, New York.

Shackleton, N. J., and M. B. Cita (1979), Oxygen and carbon isotope stratigraphy of benthic foraminifers at Site 397: Detailed history of climatic change during the late Neogene, *Initial Rep. Deep Sea Drill. Proj.*, *47*, 433–445.

Shackleton, N. J., and M. A. Hall (1984), Oxygen and carbon isotope stratigraphy of Deep Sea Drilling Project hole 552A: Plio-Pleistocene glacial history, *Initial Rep. Deep Sea Drill. Proj.*, *81*, 599–609.

Shackleton, N. J., and N. D. Opdyke (1977), Oxygen isotope and palaeomagnetic evidence for early Northern Hemisphere glaciation, *Nature*, *270*, 216–219.

Shackleton, N. J., et al. (1984), Oxygen isotope calibration of the onset of ice-rafting and history of glaciation in the North Atlantic region, *Nature*, *307*, 620–623.

Shackleton, N. J., J. Imbrie, and N. G. Pisias (1988), The evolution of oceanic oxygen-isotope variability in the North Atlantic over the past three million years, *Philos. Trans. R. Soc. London, Ser. B*, *318*, 679–686.

Shackleton, N. J., A. L. Berger, and W. R. Peltier (1990), An alternative astronomical calibration of the lower Pleistocene timescale based on ODP Site 677, *Trans. R. Soc. Edinburgh Earth Sci.*, *81*, 251–261.

Shackleton, N. J., M. A. Hall, and D. Pate (1995a), Pliocene stable isotope stratigraphy of Site 846, *Proc. Ocean Drill. Program Sci. Results*, *138*, 337–355.

Shackleton, N. J., S. Crowhurst, T. Hagelberg, N. G. Pisias, and D. A. Schneider (1995b), A new late Neogene time scale: Application to Leg 138 sites, *Proc. Ocean Drill. Program Sci. Results*, *138*, 73–101.

Shipboard Scientific Party (1992), Site 846, *Proc. Ocean Drill. Program Initial Rep.*, *138*, 265–333.

Sigman, D. M., S. L. Jaccard, and G. H. Haug (2004), Polar stratification in a cold climate, *Nature*, *428*, 59–63.

Sloan, L. C., T. J. Crowley, and D. Pollard (1996), Modeling of middle Pliocene climate with the NCAR GENESIS general circulation model, *Mar. Micropaleontol.*, *27*, 51–61.

Spicer, R. A., N. B. W. Harris, M. Widdowson, A. B. Herman, S. Guo, P. J. Valdes, J. A. Wolfe, and S. P. Kelley (2003), Constant elevation of southern Tibet over the past 15 million years, *Nature*, *421*, 622–624.

Thiébault, F., M. Cremer, P. Debrabant, J. Foulon, O. B. Nielsen, and H. Zimmerman (1989), Analysis of sedimentary facies, clay mineralogy, and geochemistry of the Neogene-Quaternary sediments in Site 645, Baffin Bay, *Proc. Ocean Drill. Program Sci. Results*, *105*, 83–100.

Tian, J., P. Wang, X. Cheng, and Q. Li (2002), Astronomically tuned Plio-Pleistocene benthic $\delta^{18}O$ record from South China Sea and Atlantic-Pacific comparison, *Earth Planet. Sci. Lett.*, *203*, 1015–1029.

Tiedemann, R., M. Sarnthein, and N. J. Shackleton (1994), Astronomic timescale for the Pliocene Atlantic $\delta^{18}O$ and dust flux records of Ocean Drilling Program Site 659, *Paleoceanography*, *9*, 619–638.

Tukey, J. W. (1977), *Exploratory Data Analysis*, 688 pp., Addison-Wesley, Boston, Mass.

Venz, K. A., and D. A. Hodell (2002), New evidence for changes in Plio-Pleistocene deep water circulation from Southern Ocean ODP Leg 177 Site 1090, *Palaeogeogr. Palaeoclimatol. Palaeoecol.*, *182*, 197–220.

Walter, R. C., P. C. Manega, R. L. Hay, R. E. Drake, and G. H. Curtis (1991), Laser-fusion $^{40}Ar/^{39}Ar$ dating of Bed I, Olduvai Gorge, Tanzania, *Nature*, *354*, 145–149.

Whitman, J. M., and W. H. Berger (1992), Pliocene-Pleistocene oxygen isotope record Site 586, Ontong Java Plateau, *Mar. Micropaleontol.*, *18*, 171–198.

Willis, K. J., A. Kleczkowski, K. M. Briggs, and C. A. Gilligan (1999), The role of sub-Milankovitch climatic forcing in the initiation of the Northern Hemisphere glaciation, *Science*, *285*, 568–571.

Wilson, D. S. (1993), Confirmation of the astronomical calibration of the magnetic polarity timescale from sea-floor spreading rates, *Nature*, *364*, 788–790.

Wolf-Welling, T. C. W., M. Cremer, S. O'Connell, A. Winkler, and J. Thiede (1996), Cenozoic Arctic gateway paleoclimate variability: Indications from changes in coarse-fraction composition, *Proc. Ocean Drill. Program Sci. Results*, *151*, 515–567.

Zhisheng, A., J. E. Kutzbach, W. L. Prell, and S. C. Porter (2001), Evolution of Asian monsoons and phased uplift of the Himalaya-Tibetan plateau since late Miocene times, *Nature*, *411*, 62–66.

M. Mudelsee, Institute of Meteorology, University of Leipzig, Stephanstrasse 3, 04103 Leipzig, Germany. (mudelsee@uni-leipzig.de)

M. E. Raymo, Department of Earth Sciences, Boston University, 685 Commonwealth Avenue, Boston, MA 02215, USA.